

Preprint: in *Local Structure from Diffraction Materials*
Science Research Series eds. M.F. Thorpe and S. Billinge
(Plenum Press) New York (1998)

LOCAL ATOMIC ARRANGEMENTS IN BINARY SOLID SOLUTIONS STUDIED BY X-RAY AND NEUTRON DIFFUSE SCATTERING FROM SINGLE CRYSTALS

J. L. Robertson,¹ C. J. Sparks,¹ G. E. Ice,¹ X. Jiang,¹ S. C. Moss,²
and L. Reinhard³

¹Oak Ridge National Laboratory, Oak Ridge, TN 37831 USA

²University of Houston, Houston, TX 77204 USA

³ETH Zentrum, CH-8092 Zurich Switzerland

INTRODUCTION

The concepts of order and disorder are fundamental to understanding the many physical properties exhibited by various materials. In general, these concepts are quite ambiguous, but when applied to a particular circumstance, they often provide needed insight into the relationship between how the atoms are arranged locally in a material and its bulk properties. Examples include phase stability, electrical resistance and magnetism. In addition, the notion of order vs. disorder applies equally to equilibrium and non-equilibrium systems. It is interesting to note that a chemically disordered material can indeed be the equilibrium phase over a large range of temperature, pressure and composition. This phenomenon can be best understood by considering the competition between short-range and long-range ordering tendencies (which can be incompatible with one another) together with the constant rearrangement of the atoms resulting from thermal diffusion (entropy) at elevated temperatures. Figure 1 shows the FeCr binary alloy phase diagram¹ where the entire phase field denoted as (Fe,Cr) represents a chemically disordered structure as the equilibrium phase.

In this paper, we will be concerned with local atomic arrangements in crystalline binary solid solutions and how information about the local order can be obtained from diffuse x-ray and neutron scattering measurements.² For the purposes of this paper, a binary solid solution should be thought of as a crystal lattice decorated by two atomic species, labeled A and B, which occupy the atomic sites in such a way that there is no long-range order. In other words, there is no overall pattern that determines which kind of atom, A or B, will occupy a particular atomic

site. The crystal lattice is assumed to be either simple face-centered cubic (fcc) with four atoms per unit cell or simple body-centered cubic (bcc) with two atoms per unit cell. However, the methods presented here can, with some difficulty, be generalized to include other lattice symmetries.³ These methods can also be applied to extremely complex crystals in cases where only a small subset of the atomic sites are chemically disordered.

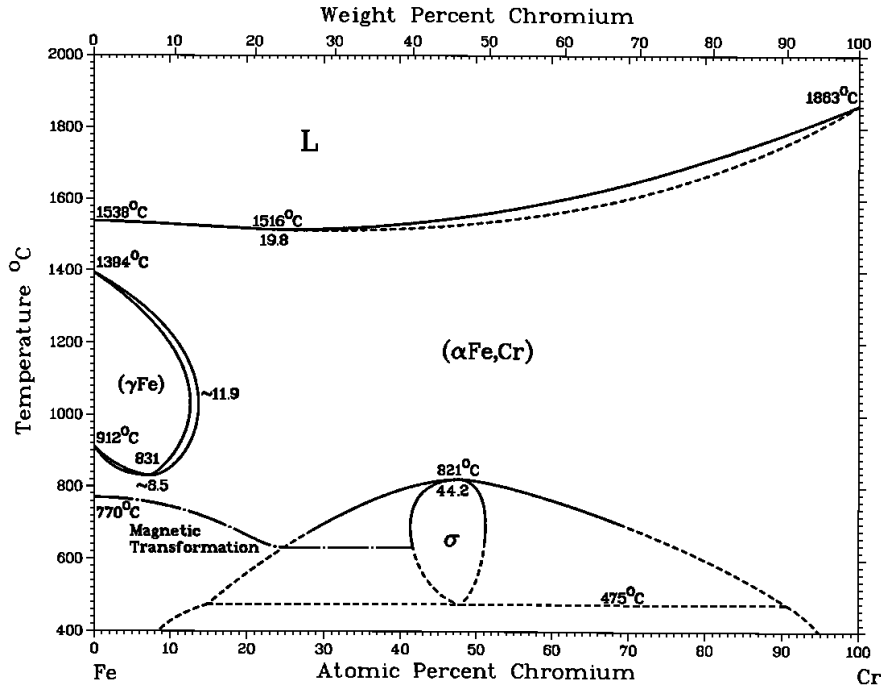


Figure 1. Alloy phase diagram for the Fe-Cr system.²

In the development that follows the amount of order present in a system is defined relative to a completely disordered alloy. In such a reference alloy the probability distribution describing which atomic species will occupy a particular atomic site is simply given by the composition. For example, suppose a lattice is composed of half A atoms and half B atoms. The chance of finding an A atom on a given site is 50% and the chance of finding a B atom there is also 50%. If the composition had been A₂₀B₈₀ then there would be a 20% chance for an A atom and a 80% chance for a B atom to occupy a given atomic site. However, such an ideally disordered state is almost never realized in real alloys. The type of atom occupying a particular site invariably influences the distribution of atomic species on neighboring sites due to electronic and/or magnetic interactions, atomic size mismatch, etc. This of course introduces short-range correlations in the chemical order – also referred to as concentration fluctuations in the formalism developed by Krivoglaz.⁴ There are two distinct ordering tendencies that can arise from these short-range chemical correlations. The first occurs if the probability of finding unlike pairs of atoms occupying adjacent atomic sites is greater than what would be expected in a completely random alloy with the same composition. This type of order, if extended to include longer-range correlations, would ultimately lead to the formation of a superlattice structure and

is usually referred to as atomic short-range order. If, on the other hand, the atoms on neighboring atomic sites are more likely to be of the same atomic species, then the system will tend toward phase separation. This type of concentration fluctuations is referred to as clustering.

Atomic displacements (local static, or frozen, deviations of the atoms from their ideal lattice sites) usually accompany the concentration fluctuations found in binary solid solutions. These displacements violate the lattice symmetry locally but the (cubic) symmetry of the lattice as a whole must be preserved. For example, consider the addition of a small number of large atoms, labeled A, to a lattice of smaller atoms, labeled B. The lattice will be expanded around the A atoms which increases the lattice parameter from the value expected for a lattice of only B atoms. This introduces the concept of the average lattice where every atom in the crystal can be thought of as being displaced by a small amount relative to an undistorted lattice. The lattice parameter for the solid solution is then taken to be that of the average lattice, which turns out to be the value one would get by averaging over all of the unit cells in the crystal. What this simple picture implies is that AA near neighbor pairs will have a greater separation than that expected from the lattice parameter and BB near neighbor pairs will have a smaller separation. In general, a nearly linear response of the lattice parameter to the concentration (e.g. the addition of A atoms) throughout the solubility range is observed. This is Vegard's Law.⁵ The variation of the lattice parameter with concentration in substitutional alloying is a long-range effect and has been well characterized. The local or near neighbor displacements, however, are not well understood. The local effect of atomic size is crucial to understanding the behavior of substitutional alloys since atomic size disparity between the solvent and solute atoms is known to affect solubility as well as the physical and chemical properties of the alloy. Several theoretical models have been proposed to explain the linear relationship between the lattice parameter and concentration.⁵⁻⁷ While these models reproduce the almost linear change in lattice parameter with concentration, accurate measurements of the local atomic displacements to test these models on an atomic scale are almost non-existent.

SCATTERING THEORY

As was mentioned above, the diffuse scattering from crystalline solid solutions is sensitive to both the local concentration fluctuations and static atomic displacements. Several methods⁸⁻¹⁰ have been developed to extract the desired information from the diffuse scattering data and the development presented here borrows from all of them. Let us begin with intensity at a given scattering vector \mathbf{Q} for a binary alloy expressed by

Where $|\mathbf{Q}| = 4\pi\sin(\theta)/\lambda$, f_p and f_q denote the complex atomic scattering factor for x-rays or the

$$I(\mathbf{Q}) = \sum_p \sum_q f_p f_q e^{i\mathbf{Q} \cdot (\mathbf{r}_p - \mathbf{r}_q)}. \quad (1)$$

atomic scattering lengths for neutrons, the indices p and q designate lattice sites such that each sum runs over every atom in the crystal, and \mathbf{r}_p and \mathbf{r}_q are the position vectors for those sites. For crystals where the Bragg reflections are sharp and the average lattice is well-defined, the atomic positions can be represented by $\mathbf{r} = \mathbf{R} + \delta$ where \mathbf{R} is a lattice vector of the average lattice and δ is the displacement of the atom from that lattice site. The exponential in Eq. 1 can then be written as

$$e^{i\mathbf{Q} \cdot (\mathbf{r}_p - \mathbf{r}_q)} \dots e^{i\mathbf{Q} \cdot [(\mathbf{R}_p + \mathbf{a}_p) - (\mathbf{R}_q + \mathbf{a}_q)]} \dots e^{i\mathbf{Q} \cdot [(\mathbf{R}_p - \mathbf{R}_q) + (\mathbf{a}_p - \mathbf{a}_q)]} \dots e^{i\mathbf{Q} \cdot (\mathbf{R}_p - \mathbf{R}_q)} e^{i\mathbf{Q} \cdot (\mathbf{a}_p - \mathbf{a}_q)} \quad (2)$$

and the exponential involving the displacements, δ , can be expanded as

$$e^{i\mathbf{Q} \cdot (\mathbf{a}_p - \mathbf{a}_q)} \dots 1 + i\mathbf{Q} \cdot (\mathbf{a}_p - \mathbf{a}_q) - \frac{[\mathbf{Q} \cdot (\mathbf{a}_p - \mathbf{a}_q)]^2}{2!} + \dots + i^j \frac{[\mathbf{Q} \cdot (\mathbf{a}_p - \mathbf{a}_q)]^j}{j!} + \dots, \quad (3)$$

where j is an integer. This series converges rapidly when $\mathbf{Q} \cdot (\delta_p - \delta_q)$ is sufficiently small.

The total intensity can be separated into the scattering from the average lattice I_{Bragg} and the scattering that arises from the deviations from the average lattice I_{Diffuse} . The diffuse scattering can further be broken down into contributions from the chemical short-range order and displacements. Thus by substituting Eqs. 2 and 3 into Eq. 1 we have

$$I_{\text{Total}} = I_{\text{Bragg}} + I_{\text{SRO}} + I_{\text{ISD}} + I_{\text{HOT}}. \quad (4)$$

I_{Bragg} and I_{SRO} correspond to the first term in the expansion shown in Eq. 3, I_{ISD} to the second term, $(i\mathbf{Q} \cdot (\delta_p - \delta_q))$, and I_{HOT} the remaining higher order terms. Following the treatment of Warren and co-workers^{8,9,11,12} these terms can be written, in electron units per atom, as follows for a crystal with cubic symmetry

$$I(\mathbf{Q})_{\text{Bragg}} = |c_A f_A + c_B f_B|_{p,q}^2 e^{i\mathbf{Q} \cdot (\mathbf{R}_p - \mathbf{R}_q)}; \quad (5)$$

$$\frac{I(\mathbf{Q})_{\text{SRO}}}{N} = N c_A c_B |f_A - f_B|_{lmn}^2 \tilde{a}_{lmn} e^{-2M\tilde{O}_{lmn}} \cos[\tilde{\partial}(h_1 \ell + h_2 m + h_3 n)] \quad (6)$$

$$\frac{I(\mathbf{Q})_{\text{ISD}}}{N} = N c_A c_B |f_A - f_B|_{lmn}^2 \tilde{a}_{lmn} \sin[\tilde{\partial}(h_1 \ell + h_2 m + h_3 n)] \quad (7)$$

Here N is the total number of atoms in the crystal, c_A is the concentration of A atoms, c_B is the concentration of B atoms, ℓmn are the Cartesian coordinates¹³ of the lattice vector $\mathbf{R} = \underline{(\mathbf{a}_1 \ell + \mathbf{a}_2 m + \mathbf{a}_3 n)}$ where a is the cubic lattice parameter) in units of the lattice parameter so that the single sum over ℓmn replaces the double sum over p and q , and h_1 , h_2 , and h_3 are the Cartesian coordinates of the reciprocal lattice vector ($\mathbf{Q} = \pi/2 \times (\mathbf{b}_1 h_1 + \mathbf{b}_2 h_2 + \mathbf{b}_3 h_3)$ where b is the reciprocal space lattice constant). In the case of a purely random alloy, $I_{\text{SRO}}(\mathbf{Q})$ would be given by

$$I_{\text{SRO}}(\mathbf{Q}) = c_A c_B |f_A - f_B|^2 \quad (8)$$

where $\text{Re}()$ denotes the real part of the ratio of complex scattering factors. It should be noted that it is the individual components of the displacements that are averaged of all the symmetry equivalent pairs in the crystal such that

$$Q \langle \ddot{A}_{lmn}^{AA} \rangle = \frac{2\partial}{a} \left(h_1 \langle \ddot{A}_{lmn}^{AA} \rangle + h_2 \langle \ddot{A}_{lmn}^{AA} \rangle + h_3 \langle \ddot{A}_{lmn}^{AA} \rangle \right) \quad (11a)$$

and

$$Q \langle \ddot{A}_{lmn}^{BB} \rangle = \frac{2\partial}{a} \left(h_1 \langle \ddot{A}_{lmn}^{BB} \rangle + h_2 \langle \ddot{A}_{lmn}^{BB} \rangle + h_3 \langle \ddot{A}_{lmn}^{BB} \rangle \right). \quad (11b)$$

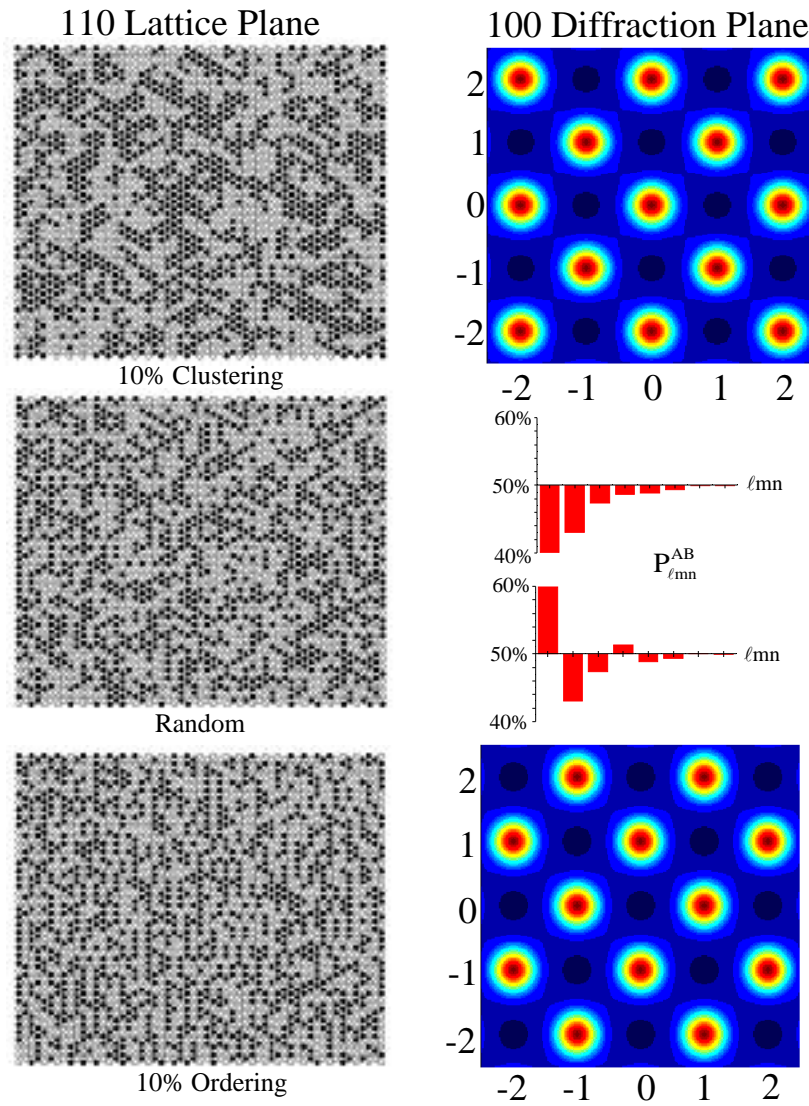


Figure 2. Direct and reciprocal space representations for a clustering, a random, and an ordering $A_{50}B_{50}$ bcc alloy.

The existence of an average lattice requires that the weighted average of the displacements for all AA, AB, BA, and BB pairs for each coordination shell must be zero. Thus, given that the $\ddot{\mathbf{A}}_{lmn}^{AB} = \ddot{\mathbf{A}}_{lmn}^{BA}$ displacement terms involving AB pairs have been removed from Eq. 10 by applying the average lattice constraint

$$\ddot{\mathbf{A}}_{lmn}^{AB} = \frac{1}{2(\dot{a}_{lmn} - 1)} \frac{-\mathbf{e}_A}{c_B} + \dot{a}_{lmn} \sqrt{\ddot{\mathbf{A}}_{lmn}^{AA}} + \frac{-\mathbf{e}_A}{c_B} + \dot{a}_{lmn} \sqrt{\ddot{\mathbf{A}}_{lmn}^{BB}} . \quad (12)$$

No assumption has been made as to how the displacements are distributed about the average. This information is contained in $I_{HOT}(\mathbf{Q})$. In order to evaluate $I_{HOT}(\mathbf{Q})$ we make the assumption that either the quadratic and higher order terms in the series expansion of the thermal and static displacements are the same for AA, AB and BB atom pairs or that the different elements have nearly the same atomic scattering factors.¹⁵⁻¹⁸ If either of these assumptions is valid we can write $I_{HOT}(\mathbf{Q})$ as

$$I_{HOT}(\mathbf{Q}) = \int_j |c_A f_A + c_B f_B|^2 \frac{j^j}{j!_{lmn}} \langle (\mathbf{Q} \cdot \mathbf{a})^j \rangle e^{i\mathbf{Q} \cdot \mathbf{R}_{lmn}} + c_A c_B |f_A - f_B|^2 \frac{j^j}{j!_{lmn}} \dot{a}_{lmn} \langle (\mathbf{Q} \cdot \mathbf{a})^j \rangle e^{i\mathbf{Q} \cdot \mathbf{R}_{lmn}} . \quad (13)$$

The first term in Eq. 13 reduces the intensity of the Bragg peaks and distributes this intensity as thermal and static diffuse scattering. This corresponds to the usual Debye-Waller factor commonly used by crystallographers. The second term in Eq. 13 reduces the intensity associated with the chemical ordering. This term has been treated by Walker and Keating¹⁹ and is included as a Debye-Waller like factor $e^{-2M\Phi_{lmn}}$ in Eq. 6.

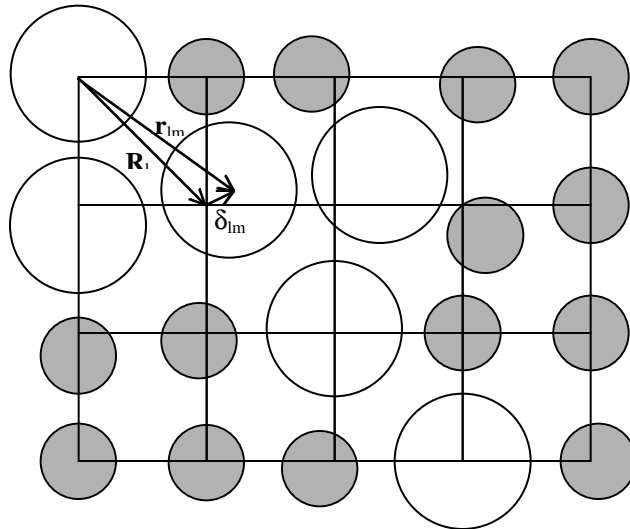


Figure 3. Schematic diagram showing a particular displacement, δ_{lmn} . It is important to remember that the displacement parameters from Eqs. 10 and 11 correspond to the average of each component of this vector over all symmetry equivalent ℓmn pairs in the crystal.

EXPERIMENTAL METHODS

In most cases the statistical quality of the data and the presence of systematic error make it difficult to recover any information from $I_{\text{HOT}}(\mathbf{Q})$. Thus the usual strategy is to try and separate the $I_{\text{SRO}}(\mathbf{Q}) + I_{\text{ISD}}(\mathbf{Q})$ contributions from $I_{\text{Total}}(\mathbf{Q})$. For diffuse neutron scattering this can be done when the data are collected by utilizing an energy analyzer to remove all but the elastic scattering from the diffracted beam. The elastic contribution to the scattering from $I_{\text{HOT}}(\mathbf{Q})$ is assumed to be small and is simply ignored.

For diffuse x-ray scattering the situation is more complicated. In the past about all one could do was to calculate the thermal diffuse scattering and subtract it from the data. More recently, the availability of x-ray synchrotron sources has made it possible to tune the incident energy of the x-rays so as to vary the scattering contrast between the two atomic species. This technique takes advantage of the anomalous dispersion that occurs when the incident x-ray energy is near an x-ray absorption edge of one of the two atomic species.¹⁰ The two contributions to $I_{\text{Total}}(\mathbf{Q})$ of interest, $I_{\text{SRO}}(\mathbf{Q})$ and $I_{\text{ISD}}(\mathbf{Q})$, are strongly dependent on the scattering contrast, $\Delta f = f_A - f_B$, see Eq. 6 and 7. Thus, one can measure the diffuse intensity at two scattering contrasts; one where Δf is large and one where Δf is small. The data where Δf is small will contain little or no contribution from $I_{\text{SRO}}(\mathbf{Q})$ or $I_{\text{ISD}}(\mathbf{Q})$ so it can be rescaled to the average scattering per atom at the x-ray energy where Δf is large and then subtracted away leaving only the contrast dependent contribution at that energy.¹⁵ The contrast dependent part of $I_{\text{HOT}}(\mathbf{Q})$ also remains, but this is taken to be small and is ignored in much the same way as for diffuse neutron scattering. In both x-ray and neutron diffraction the Bragg intensity is simply omitted since it only occurs at a few points in reciprocal space.

Once $I_{\text{SRO}}(\mathbf{Q}) + I_{\text{ISD}}(\mathbf{Q})$ has been separated from the total scattering, Eqs. 6 and 7 can be fit to the data whether it comes from x-ray or neutron diffraction. Because $I_{\text{SRO}}(\mathbf{Q})$ has even symmetry and $I_{\text{ISD}}(\mathbf{Q})$ has odd symmetry the least squares problem is well conditioned so that one should expect little or no interdependence between the $\alpha_{\ell mn}$'s and the $\gamma_{\ell mn}$'s. This is in spite of the fact that $\alpha_{\ell mn}$ appears explicitly in the expression for $\gamma_{\ell mn}$ in Eq. 10. The ‘‘coupling factors’’, $\Phi_{\ell mn}$, in Eq. 6 can be evaluated using various approximations for phonon dispersion in the alloy.^{11,20} The leading term $\Phi_{000} = 0$ for x-ray diffuse scattering where the instantaneous correlation function is measured but not for elastic neutron scattering where $\Phi_{000} \approx 1$. Typically, the approximation $\Phi_{000} \approx 1$ is also made for $\ell mn \neq 0$ for both x-rays and neutrons.²¹

With only one data set where the scattering contrast, Δf , is large one can only determine the $\gamma_{\ell mn}$'s but not the species dependent atomic displacement parameters, $\ddot{A}_{\ell mn}^{\text{AB}}$. In order to extract the species dependent parameters, at least one additional high contrast data set is required where the scattering contrast is substantially different from the first. If possible one should attempt to have $f_A > f_B$ for one contrast and $f_B > f_A$ for the other. This can be achieved with x-rays in exactly the same way as described above for large and small Δf , and by isotopic substitution using neutrons. Quite often at least one of the atomic species will not have an absorption edge within the accessible x-ray energy range available at the synchrotron, and there are no isotopes available (often they are simply too expensive) for use in a neutron diffuse scattering measurement. In this case one should consider using a combination of x-ray and neutron diffuse scattering data to get the required change in scattering contrast. Once the two large scattering contrast data sets are ready, the $\ddot{A}_{\ell mn}^{\text{AA}}$ and $\ddot{A}_{\ell mn}^{\text{BB}}$, can be obtained directly from the least squares analysis by substituting Eq. 10 into Eq. 7.

EXAMPLE: FeCr

The FeCr binary system²² exhibits a bcc solid solution (α -FeCr, see Fig. 1) over a wide temperature and concentration range. At $\sim 1100\text{K}$, a structural transformation to the σ -phase, a complex close-packed Frank-Kasper phase, occurs. According to thermodynamic evaluations^{22,23} the σ -phase decomposes below $\sim 700\text{K}$ into Fe-rich and Cr-rich bcc phases. Since the bcc to σ transformation is very sluggish, a metastable miscibility gap for α -FeCr is observed well above this decomposition temperature. One might expect the local order in the bcc phase to reveal a tendency toward phase separation. However, there is also the alternative possibility that directly above the σ -phase equilibrium boundary the local atomic arrangements might reflect the incipient σ -phase formation through premonitory fluctuations. In alloy systems such premonitory fluctuations can, for example, include atomic short-range order as well as local atomic displacements.

A single crystal of $\text{Fe}_{53}\text{Cr}_{47}$ was grown at the Materials Preparation Lab, Ames Laboratory, Iowa State University by L. L. Jones using a Bridgeman technique. The purity of the alloying elements was 99.95% and 99.996% for Fe and Cr, respectively, and the Cr concentration was determined by chemical analysis to be 47.2%. The crystal was roughly cylindrical in shape with a diameter of 12mm and a length of $\sim 20\text{mm}$. After a homogenization anneal at 1600K the crystal was held at 1108K (5K above the σ -phase transition temperature, see Fig. 1) for four days in a sealed quartz tube under a purified argon atmosphere then water-quenched. Extensive small-angle neutron scattering studies²⁴ of quenched and annealed α -FeCr alloys indicate that such a quench will preserve the high temperature equilibrium configurational order. Small angle neutron scattering was used to verify that this was the case for our sample.

The X-ray scattering experiment¹⁶ was performed on the ORNL beamline X-14A²⁵ of the National Synchrotron Light Source (NSLS) at Brookhaven National Laboratory. The measurements were done using three different energies for the incident x-rays: (i) $E=5.969\text{keV}$ (20eV below the Cr K absorption edge). This energy was chosen to maximize the scattering contrast between Cr and Fe and thus enhance the contribution from the local order in the crystal. We refer to it as the “Cr edge”. (ii) $E=7.092\text{keV}$ (20eV below the Fe K absorption edge). At this energy $f_{\text{Cr}} > f_{\text{Fe}}$, i.e. Cr becomes a stronger scatterer than Fe and we shall refer to it as the “Fe edge”. This contrast inversion affects the sign of $I_{\text{ISD}}(\mathbf{Q})$, see Eqs. 7 and 10. Therefore, a comparison of the data measured with the “Fe edge” energy with those measured with the “Cr edge” energy highlights the “size effect” scattering. (iii) $E=7.600\text{keV}$. This choice minimizes the scattering contrast whereby the $I_{\text{SRO}}(\mathbf{Q}) + I_{\text{ISD}}(\mathbf{Q})$ contribution to the total intensity are small, thus the measured intensity is predominately due to $I_{\text{Bragg}}(\mathbf{Q}) + I_{\text{HOT}}(\mathbf{Q})$. Figure 4 shows the range of contrast variation obtained during the measurement. Note the greatly enhanced $|\Delta f|^2$ at the “Cr edge” as compared with $|\Delta Z|^2 = 4$ without the anomalous dispersion, and the $|\Delta f|^2$ small for $E=7.600\text{keV}$.

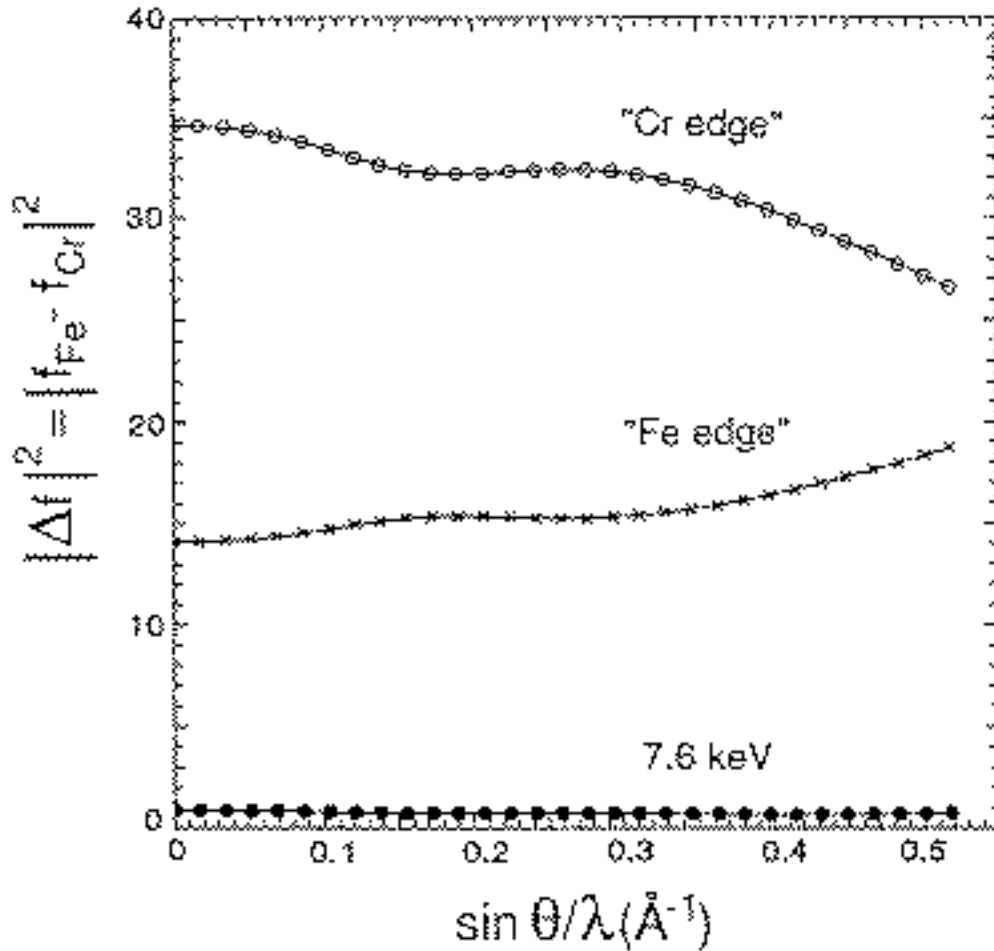


Figure 4. $|\Delta f|^2$ as a function of $\sin \theta / \lambda$ for the three x-ray energies used.

The results of the least-squares analysis are listed in Tables I and II. The first eleven α_{lmn} 's are positive indicating a preference for like neighbors (Fe-Fe and Cr-Cr pairs), i.e. this is a clustering system. For example, $\alpha_{111} = 0.16$ means that the probability of finding an Fe atom in the nearest neighbor shell of another Fe atom is 60.5% as compared to 52.8% ($=c_{\text{Fe}}$) for a totally random alloy. Given the high concentration of this alloy, the α_{lmn} are rather small and so the clustering tendency is not very pronounced. According to anomalous x-ray diffraction studies by Yankel,²⁶ σ -FeCr is partially long-range ordered, i.e. there are sublattices which are preferentially filled with Fe or Cr. For every interatomic vector connecting points in two different sublattices, the corresponding α_{lmn} must be negative. Evidently, the positive α_{lmn} 's of the bcc solid solution above T_c do not reflect the local chemical order found in the σ -phase.

From Table II we see that most of the components of $\hat{\mathbf{A}}_{lmn}^{\text{FeFe}}$ are negative. Therefore most of the average Fe-Fe separations (in particular those for the first three neighbor shells) are smaller

than the corresponding average lattice distances. This is compatible with the observed decrease of the lattice parameter with increasing Fe concentration. However, the comparatively large negative value of the nearest neighbor Cr-Cr displacement shows that the concentration dependence of the lattice parameter is not necessarily reflected in a simple way in the local atomic distortions, i.e. from Vegard's Law one would expect the first nearest neighbor displacements to be positive! Nevertheless, the \ddot{A}_{lmn}^{CrCr} are on the average more positive than the \ddot{A}_{lmn}^{FeFe} . Thus the data suggest that taken over a sufficiently large local volume, the Cr atoms are indeed "bigger" than the Fe atoms. The average Cr-Cr nearest neighbor distance is 0.4% smaller and the average Cr-Cr next nearest neighbor distance is 0.3% larger than the corresponding average lattice separations. By comparison, the lattice parameter of pure Cr is 0.6% larger than the lattice parameter of pure Fe. It is also interesting to note that the root-mean-square static displacement amounts to only about ~3% of the root-mean-square thermal displacement.

Table I. Short-range order parameters α_{lmn} .

ℓmn	α_{lmn}	ℓmn	α_{lmn}
0 0 0	1.1806(23)	3 3 3	0.0051(8)
1 1 1	0.1596(14)	5 1 1	0.0025(6)
2 0 0	0.0691(14)	4 4 0	-0.006(7)
2 2 0	0.0455(11)	5 3 1	0.0016(4)
3 1 1	0.0217(10)	4 4 2	0.0022(5)
2 2 2	0.0253(11)	6 0 0	-0.0020(8)
4 0 0	0.0036(11)	6 2 0	0.0009(4)
3 3 1	0.0074(8)	5 3 3	0.0009(4)
4 2 0	0.0074(7)	6 2 2	0.0010(4)
4 2 2	0.0043(7)	4 4 4	0.0007(7)

Table II. Species dependent displacement parameters $\Delta_{lmn} = (\Delta x_{lmn}, \Delta y_{lmn}, \Delta z_{lmn})$ in Å. The Fe-Cr displacements can be obtained from Eq. 12.

ℓmn	\ddot{A}_{lmn}^{FeFe}	\ddot{A}_{lmn}^{FeFe}	\ddot{A}_{lmn}^{FeFe}	\ddot{A}_{lmn}^{CrCr}	\ddot{A}_{lmn}^{CrCr}	\ddot{A}_{lmn}^{CrCr}
1 1 1	-0.00070 (4)	-0.00070(4)	-0.00070(4)	-0.0019(5)	-0.0019(5)	-0.0019(5)
2 0 0	-0.00029(9)	0.00000	0.00000	0.00268(12)	0.00000	0.00000
2 2 0	-0.00022(4)	-0.00022(4)	0.00000	-0.00050(6)	-0.00050(6)	0.00000
3 1 1	0.00018(5)	-0.00022(3)	-0.00022(3)	-0.00007(6)	0.00011(4)	0.00011(4)
2 2 2	-0.00053(5)	-0.00053(5)	-0.00053(5)	0.00039(6)	0.00039(6)	0.00039(6)
4 0 0	0.00009(9)	0.00000	0.00000	0.00063(13)	0.00000	0.00000
3 3 1	-0.00013(4)	-0.00013(4)	-0.00005(4)	0.00016(4)	0.00016(4)	-0.00005(6)

Figure 5 compares the measured intensities in the $(h_1, h_2, 0)$ plane (after subtracting the $E=7.600\text{keV}$ data) with those reconstructed from the from the parameters in Tables I and II. The increase in the intensity near the Bragg positions and the details of the intensity in the zone boundary regions are well reproduced. These modulations are largely due to the "size effect" scattering as can be inferred from the systematic differences between the "Cr edge" and the "Fe edge" data. For example, the "dip" near 210 in the "Cr edge" data which becomes a local

maximum in the “Fe edge” data, both of which may be related to a measurable zone boundary softness in the $[100]_L$ phonon branch.²⁷

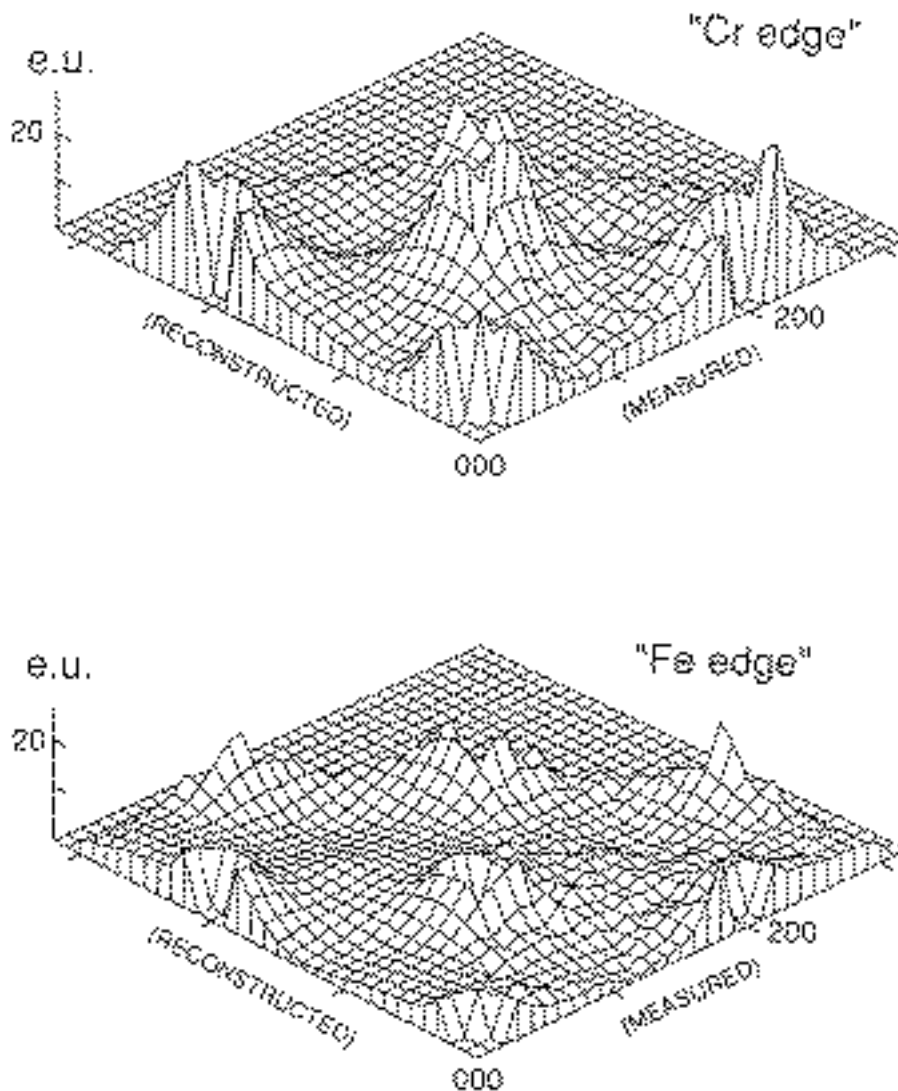
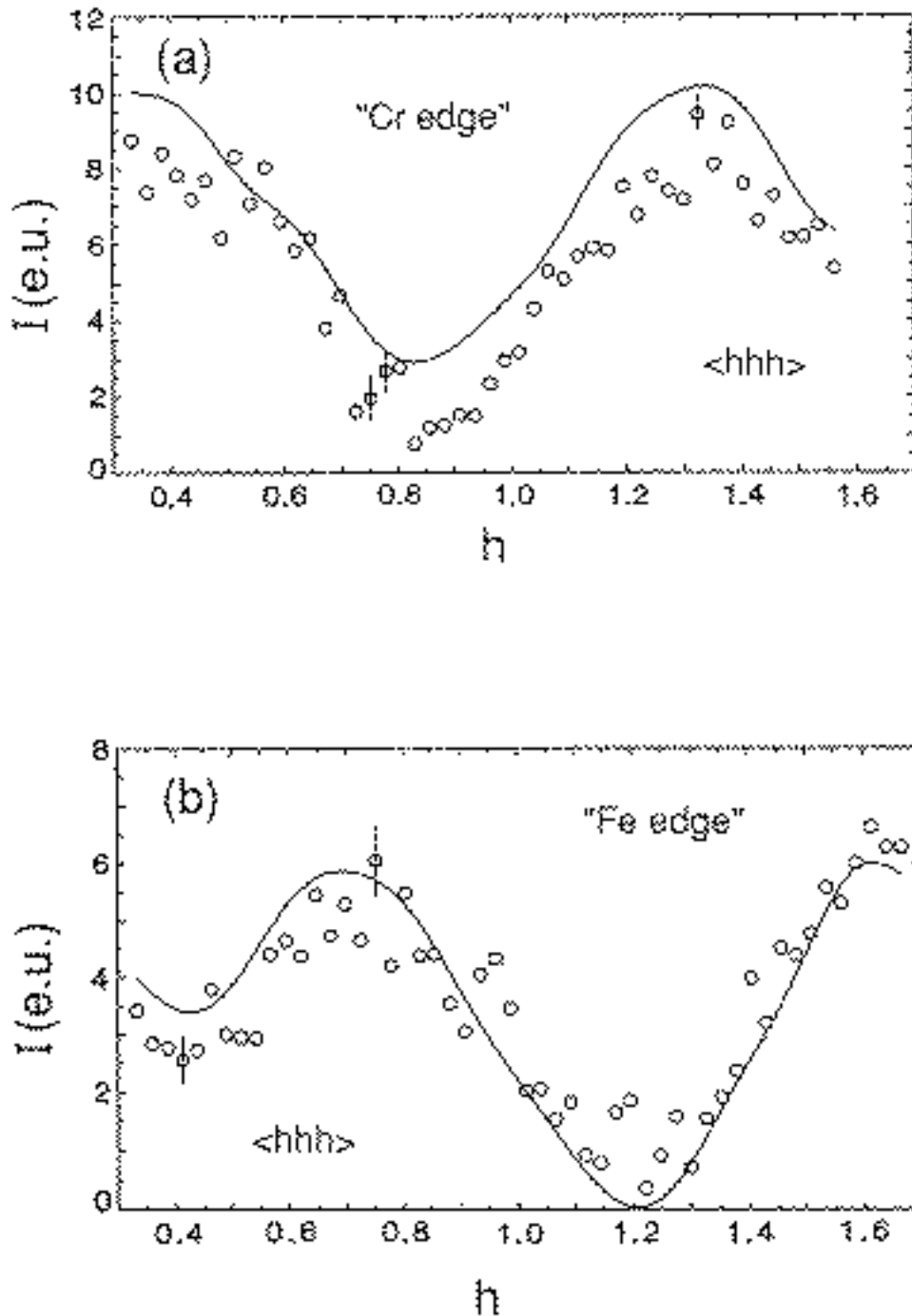


Figure 5. Measured and reconstructed intensities in the $(h_1, h_2, 0)$ plane in electron units for the “Cr edge” and “Fe edge”.

The measured intensity is compared with the results of the least-squares refinement along the $\langle hhh \rangle$ direction in Fig. 6. The intensity minimum around $h=0.8$ in the “Cr edge” data and the maximum around $h=0.7$ in the “Fe edge” data are caused by the “size effect” modulation and are related to the dip at $2/3(111)$ in the $[111]_L$ phonon branch. The difference in their positions can be explained by considering the $I_{\text{SRO}}(\mathbf{Q})$ which peaks at the origin, $h=0$, and therefore will shift a “size effect”-induced minimum towards a higher h value, whereas a maximum will be shifted towards lower h . The same arguments apply to the maximum near $4/3(111)$ in the “Cr edge” data and the corresponding minimum in the “Fe edge” data. This peaking of the static

diffuse scattering at the $2/3(111)$ and $4/3(111)$ is a direct consequence of the elastic softness of the bcc lattice in response to distortions in these directions as evidenced by the $2/3[111]$ dip in the $[111]_L$ phonon. Since the restoring force of the lattice to this particular displacement is relatively weak, the atoms are preferentially displaced in these directions. This is clear evidence for the coupling between the static displacements and the elastic response of the lattice.

Figure 6. Measured and reconstructed intensities in the $\langle hhh \rangle$ direction. (a) "Cr edge", (b) "Fe edge".



CONCLUSION

It has been demonstrated that accurate occupational probabilities and first order static displacements can be obtained from diffuse scattering measurements. It is quite remarkable that species dependent atomic displacements on the order of 0.001\AA and smaller can be determined from such broad features in the diffraction pattern. The availability of this information will provide theorists with the means to test their models and challenge them to include static displacements in their *ab initio* calculations of phase stability. In even more general terms, knowledge about the local atomic arrangements will help us to understand the connection between local structure and bulk properties.

ACKNOWLEDGEMENTS

The part of this work undertaken at Oak Ridge National Laboratory was supported by the US DOE under Contract No. DE-AC05-96OR22464 with Lockheed Martin Energy Research Corporation. The portion carried out at the University of Houston was supported by the NSF on DMR-9208450 and by the US DOE on DE-FG05-87ER45325.

REFERENCES

1. T. B. Massalski, *Binary Alloy Phase Diagrams*, American Society for Metals, Metals Park, Ohio (1986).
2. Electron diffraction measurements are also very useful for studying local atomic order. However, because the data analysis and interpretation are substantially different from x-ray and neutron scattering measurements, electron diffraction methods will not be discussed in this paper.
3. S. Hashimoto, *Acta Cryst.* A43: 481 (1987).
4. M. A. Krivoglaz, *Theory of X-Ray and Thermal Neutron Scattering from Real Crystals*, Plenum Press, New York (1969).
5. L. Vegard, *Z. Kristallogr.* 67:239 (1928).
6. C. J. Sparks, G. E. Ice, X. Jiang, and P. Zschack, *Mater. Res. Soc. Symp. Proc.* 375:213 (1975).
7. G. E. Ice, C. J. Sparks, J. L. Robertson, J. E. Epperson, and X. Jiang, *Mater. Res. Soc. Symp. Proc.* 437:181 (1996).
8. B. E. Warren, B. L. Averbach, and B. W. Roberts, *J. Appl. Phys.* 22:1493 (1951).
9. B. Borie and C. J. Sparks, *Acta Cryst.* A17:198 (1971).
10. G. E. Ice, C. J. Sparks, and L. B. Shaffer, *Resonant Anomalous X-Ray Scattering: Theory and Experiment*, ed. G. Materlik, C. J. Sparks, and K. Fischer, North Holland, Amsterdam (1994).
11. B. E. Warren, *X-Ray Diffraction*, Dover, New York (1969).
12. J. M. Cowley, *J. Appl. Phys.* 21:24 (1950).
13. By convention the indices lmn have been multiplied by two so that they are all integers hence the factor of $\frac{1}{2}$ in the expression for \mathbf{R} .
14. V. Gerold and J. Kern, *Acta Metall.* 35:393 (1987).

15. G. E. Ice, C. J. Sparks, A. Habenschuss, and L. B. Shaffer, *Phys. Rev. Lett.* 68:863 (1992).
16. L. Reinhard, J. L. Robertson, S. C. Moss, G. E. Ice, P. Zschack, and C. J. Sparks, *Phys. Rev. B* 45:2662 (1992).
17. B. Schönfeld, G. E. Ice, C. J. Sparks, H. G. Haubold, W. Schweika, and L. B. shaffer, *Phys. Status Solidi B* 183:79 (1989).
18. X. Jiang, G. E. Ice, C. J. Sparks, J. L. Robertson, and P. Zschack, *Phys. Rev. B* 57:3211 (1995).
19. C. B. Walker and D. T. Keating, *Acta Cryst.* 14:1170 (1961).
20. R. O Williams, *Oak Ridge National Laboratory Report No. ORNL-4848* (1972).
21. P. Gerogopoulos and J. B. Cohen, *J. Physique Colloque* 12:C7-191 (1977).
22. O. Kubaschewski, *Iron Binary Phase Diagrams*, Springer, Berlin, (1982).
23. S. Hertzmanand and B. Sundman, *CALPHAD* 6:67 (1982).
24. M. Furusaka, Y. Ishikawa, S. Yamaguchi, and Y. Fujino, *J. Phys. Soc. Jpn.* 55:2253 (1986).
25. A. Habenschuss, G. E. Ice, C. J. Sparks, and R. A. Neiser, *Nucl. Inst. And Meth. Phys. Res.* A266:215 (1988).
26. H. L. Yankel, *Acta Cryst.* B39:0 (1982).
27. J. L. Robertson, L. Reinhard, D. A. Neumann, and S. C. Moss, *Mater. Res. Soc. Symp.Proc.* 376:689 (1995).